Journal of Hazardous Materials 379 (2019) 120770

Contents lists available at ScienceDirect

Journal of Hazardous Materials

journal homepage: www.elsevier.com/locate/jhazmat

Source inversion of both long- and short-lived radionuclide releases from the Fukushima Daiichi nuclear accident using on-site gamma dose rates

Xinpeng Li[a], Sida Sun[a], Xiaofeng Hu[b], Hong Huang[c], Hong Li[a], Yu Morino[d], Shuntan Wang[a], Xingtuan Yang[a], Jiasong Shi[e], Sheng Fang[a,*]

[a] Institute of Nuclear and New Energy Technology, Collaborative Innovation Centre of Advanced Nuclear Energy Technology, Key Laboratory of Advanced Reactor Engineering and Safety of Ministry of Education, Tsinghua University, Beijing, 100084, China
[b] School of Information Technology and Network Security, People's Public Security University of China, Beijing, 100038, China
[c] Institute of Public Safety Research, Department of Engineering Physics, Tsinghua University, Beijing, 100084, China
[d] National Institute for Environmental Studies, 16-2 Onogawa, Tsukuba, 305-8506, Japan
[e] Research Institute of Chemical Defense, Beijing, 100000, China

ARTICLE INFO

Keywords:
Multi-radionuclide source term
Fukushima Daiichi accident
On-site gamma dose rate
Ensemble Kalman filter

ABSTRACT

Following a nuclear accident, on-site gamma dose rates provide the most complete record of atmospheric releases of both long- and short-lived radionuclides. However, they are seldom used for source inversion, because the radionuclide composition is unknown. This prevents the estimation of short-lived radionuclide releases. In this study, a method using on-site gamma dose rates is developed with the aim of determining the source term, including both long- and short-lived radionuclides. To reduce the uncertainties involved in source inversion, the proposed method uses reactor physics to obtain an a priori radionuclide composition and a reverse source term estimate as an a priori release rate. A weighted additive model is derived to handle the conflicts between the priors from different mechanisms and simultaneously incorporate them into the source inversion. The proposed method is applied to the Fukushima Daiichi accident and validated against both the on-site gamma dose rates and the regional measurements of Cs-137. The results demonstrate that the resolved a posteriori source term combines the advantages of both priors and substantially improves the predictions of the on-site gamma dose rates. Given a detailed a priori release rate, this approach also improves the regional predictions of both airborne and deposited Cs-137 concentrations.

1. Introduction

Large volumes of various radionuclides were released into the environment following the Fukushima Daiichi Nuclear Power Plant (FDNPP1) accident, which was induced by a strong earthquake and tsunami off the coast of Japan on March 11, 2011. The short-lived radionuclides released in the aftermath of the accident are known to make a considerable contribution to acute health hazards, whereas the long-lived radionuclides cause long-term environmental pollution [1]. Therefore, the temporal release profile of both long- and short-lived radionuclides, i.e., the source term, is a key factor in the nuclear emergency response and consequence evaluation [2]. To determine information about the release, many source inversion methods have been applied, including both inverse modeling [3–5] and reverse estimation [6–8].

However, most of these methods provide source terms for only a few (up to five) long-lived radionuclides, because they mainly rely on regional measurements acquired far away from the release position [3,7–9], and the short-lived radionuclides have decayed after such long-range transport [10,11]. In addition, the long-range transport and sparsity of remote measurements introduce uncertainties into the regional measurements, which may ultimately lead to biases in the release rate estimates [3].

In contrast, on-site gamma dose rates are acquired within the boundary of the nuclear power plant site. These dose rates quickly respond to any release, and register the contribution of both long- and short-lived radionuclides. Thus, the on-site gamma dose rates may be useful for multi-radionuclide source term estimation and could help to refine the temporal estimate of the release rate.

Unfortunately, neither inverse modeling nor reverse estimation uses on-site gamma dose rates as the primary input data, because the unknown radionuclide composition introduces considerable uncertainties

* Corresponding author.
E-mail address: fangsheng@tsinghua.edu.cn (S. Fang).

https://doi.org/10.1016/j.jhazmat.2019.120770
Received 11 January 2019; Received in revised form 15 May 2019; Accepted 12 June 2019
Available online 12 June 2019
0304-3894/

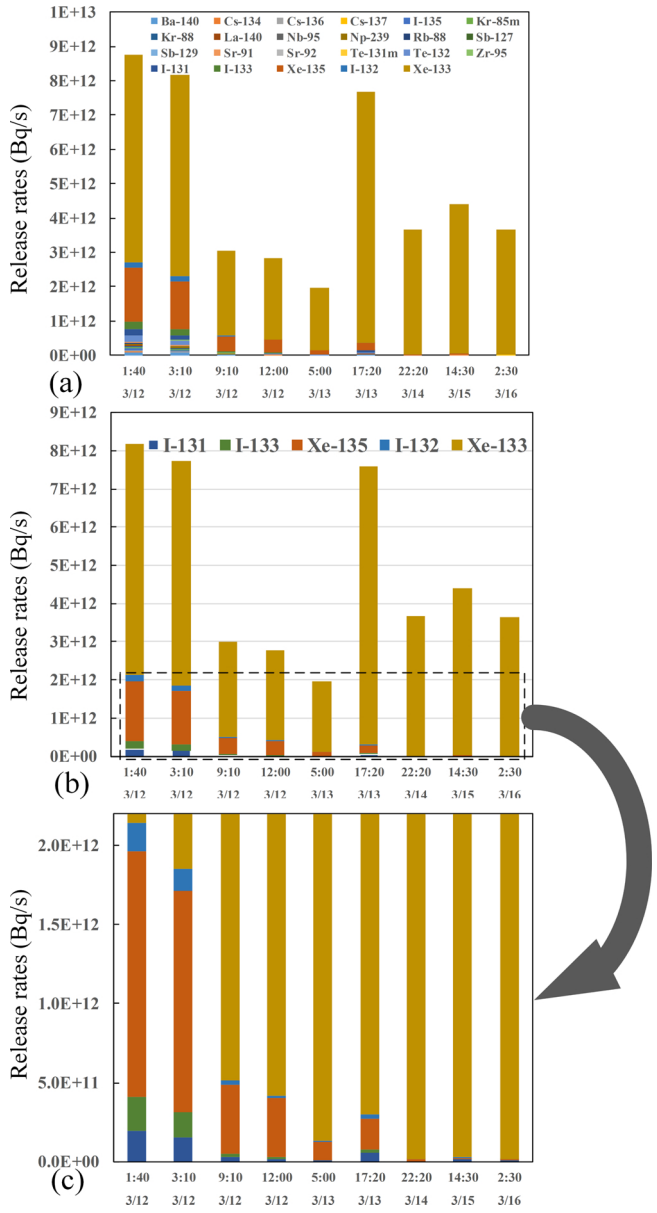

Fig. 1. Radionuclide composition of the major radionuclides (calculated using RASCAL). (a) RASCAL source term. (b) major five radionuclides. (c) Magnification of part (b).

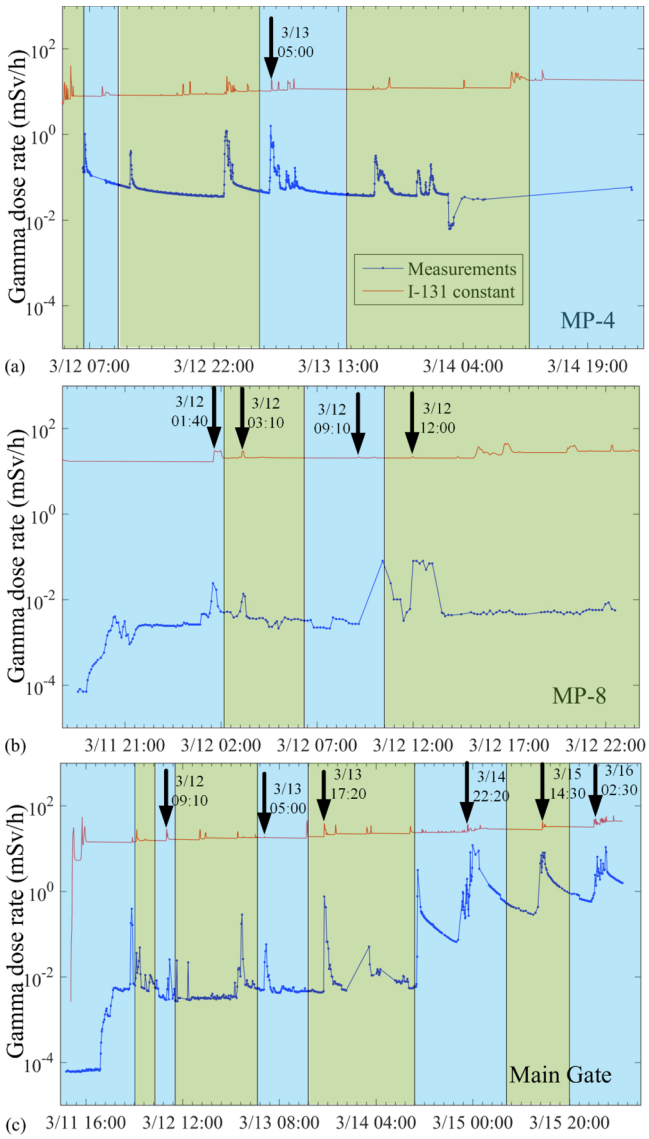

Fig. 2. Measured gamma dose rates and predicted dose rates using a constant source term. (a) MP-4; (b) MP-8; (c) Main gate. The arrows indicate the peak data that were selected for source inversion in this study (For interpretation of the references to colour in this figure legend, the reader is referred to the web version of this article).

to the source inversion process [3,7]. Instead, the on-site gamma dose rates are only used to allocate an existing total release estimate to different time sections [12] or as a supplement to regional data for the source term estimation of I-131 and Cs-137 (when insufficient regional data are available) [7]. This strategy avoids the uncertainties associated with on-site dose rate data, but also sacrifices the opportunity for source term estimation of both long- and short-lived radionuclides.

To obtain a source term including both long- and short-lived radionuclides, this study developed a source inversion method that uses the on-site gamma dose rates as fundamental input data. This method considers reactor physics to calculate the a priori composition of both long- and short-lived radionuclides, and employs a reverse source term estimate as the a priori release rate. Because these two priors come from different mechanisms, they include conflicting information. To handle this conflict, the standard inverse model is split into a weighted additive model, which allows both priors to be simultaneously incorporated into the estimation. The proposed method has been applied to the FDNPP1 accident and validated against both the on-site gamma dose rates and the regional atmospheric concentration and ground deposition measurements of Cs-137. The performance of the a posteriori multi-radionuclide source term was compared with the two a priori source terms to provide validations at both scales.

2. Methods

2.1. Inverse modeling for multi-radionuclide source term

In the framework of inverse modeling, the relationship between the dose rate measurements and the release rate can be described as:

$$\boldsymbol{\mu} = \mathbf{A}\mathbf{z} \tag{1}$$

where $\boldsymbol{\mu} \in \mathbb{R}^O$ is a vector of measurements and O is the total number of measurements, which is the product of the number of sites (m) and the number of time steps (N). The objective is to find $\mathbf{z} \in \mathbb{R}^P$, a vector containing the release rates of n radionuclides at N different times ($P = n \times N$). $\mathbf{A} \in \mathbb{R}^{O \times P}$ is the transport matrix representing the sensitivity of a measurement to the release rate of each radionuclide. Using

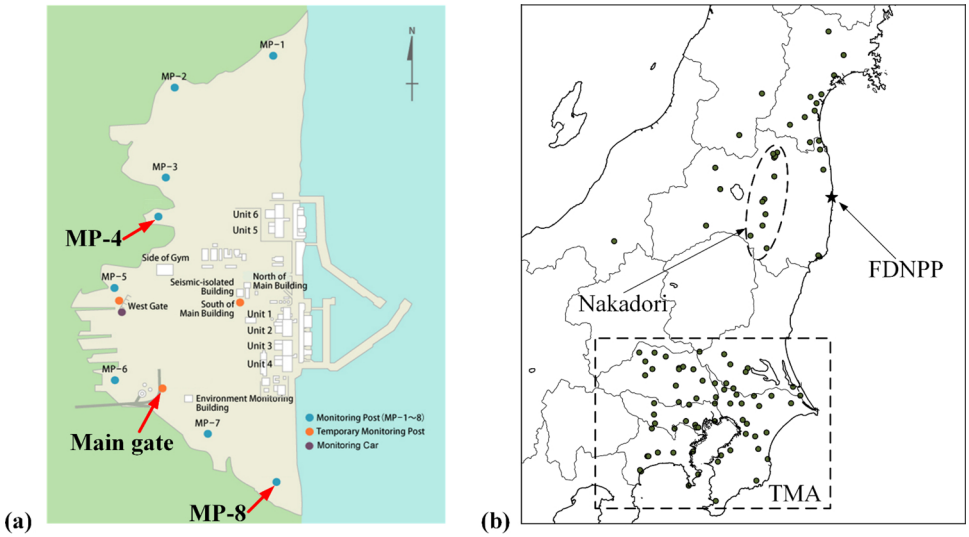

Fig. 3. Calculation domain and locations of (a) on-site gamma dose rate observation sites [30] and (b) regional suspended particulate matter observation sites. The red arrows indicate the sites involved in source inversion in this study. The dashed circle and rectangle mark the two zones of Nakadori and the Tokyo metropolitan area (TMA) [31] (For interpretation of the references to colour in this figure legend, the reader is referred to the web version of this article).

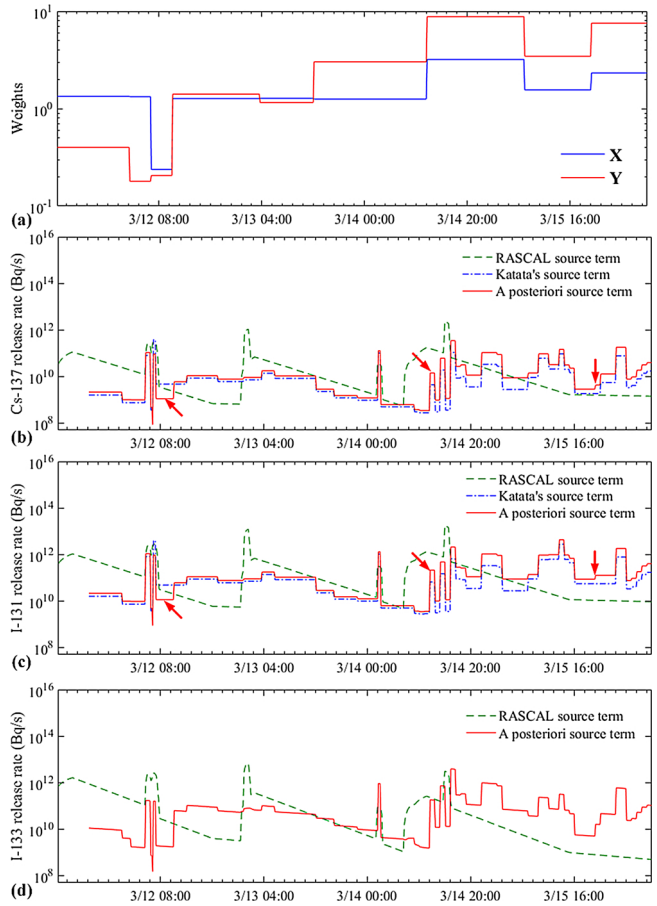

Fig. 4. Comparison of the a posteriori source term with the results of RASCAL and Katata's source term. (a) Weights for the whole period; (b) Cs-137 release rate; (c) I-131 release rate; (d) I-133 release rate. The arrows in parts (b) and (c) indicate that the details are different from Katata's estimate.

one of the released radionuclides as a reference, the composition of the radionuclides in $\mathbf{z}$ can be represented by the ratios between the other radionuclides and the reference. Without loss of generality, Cs-137 is chosen as the reference radionuclide in this study. Thus, Eq. (1) can be rewritten as:

$$\boldsymbol{\mu} = \mathbf{A}(\mathbf{R}\bullet\mathbf{c}) \tag{2}$$

where $\mathbf{R} \in \mathbb{R}^{P\times N}$ is a matrix containing the release rate ratios between different radionuclides and Cs-137 at different times and $\mathbf{c} \in \mathbb{R}^{N}$ is a vector containing the temporal release rates of Cs-137. Because the gamma dose rates do not provide any radionuclide information, both the radionuclide composition ($\mathbf{R}$) and the release rate of the reference radionuclide ($\mathbf{c}$) are unknown variables. This makes Eq. (2) a highly underdetermined problem, so a priori information of both variables is needed to obtain a reasonable solution.

2.2. Weighted additive model for priors from different mechanisms

The currently available priors for solving Eq. (2) are the source term estimates given by a reactor physics calculation and by source inversion. The former provides both short- and long-lived radionuclide compositions, but a less detailed release rate. The latter only covers a few long-lived radionuclides, but provides a more refined release rate. Therefore, we attempt to combine the radionuclide information from the reactor physics calculation with the release rate given by source inversion to solve Eq. (2). However, this combination is not straightforward, because these two priors have different radionuclide compositions and temporal resolutions.

To handle this conflict and incorporate these two priors into the estimation, the radionuclide composition in Eq. (2) is split into two groups and the following weighted additive model is proposed:

$$\boldsymbol{\mu} = \mathbf{A}(\mathbf{R}_{Inv}\mathbf{X} + \mathbf{R}_{Rea}\mathbf{Y})\bullet\mathbf{c}_{Inv} \tag{3}$$

where $\mathbf{R}_{Inv} \in \mathbb{R}^{P\times N}$ and $\mathbf{R}_{Inv} = [\mathbf{R}_1, \mathbf{R}_2, ..., \mathbf{R}_k, 0, ..., 0]^T$ is the composition matrix of the first radionuclide group, which includes the k radionuclides that are common to the estimates from both the reactor physics calculation and source inversion. $\mathbf{R}_i = diag(r_{i1}, r_{i2}, r_{i3}, ..., r_{iN})$ is the diagonal matrix containing the release rate ratios between the i-th radionuclide and Cs-137 at different times. These radionuclides have relatively long half-lives, so their composition can be measured and $\mathbf{R}_{Inv}$ is determined by the source inversion estimate. $\mathbf{R}_{Rea} = [0, 0, ..., 0, \mathbf{R}_{k+1}, \mathbf{R}_{k+2}, ..., \mathbf{R}_n]^T$ is the composition matrix of the second radionuclide group, which includes the remaining radionuclides that only appear in the estimate from the reactor physics calculation. These radionuclides are often short-lived, so there are no corresponding measurements and $\mathbf{R}_{Rea}$ is set according to the reactor physics calculation. $\mathbf{c}_{Inv} \in \mathbb{R}^{N}$ is the a priori release rate of Cs-137 given by the source inversion method. $\mathbf{X} = diag(x_1, x_2, x_3, ..., x_N)$ and $\mathbf{Y} = diag(y_1, y_2, y_3, ..., y_N)$ are two unknown weights that correct the a priori release rate for each radionuclide group.

After solving $\mathbf{X}$ and $\mathbf{Y}$ from Eq. (3), the final multi-radionuclide source term estimate is given by:

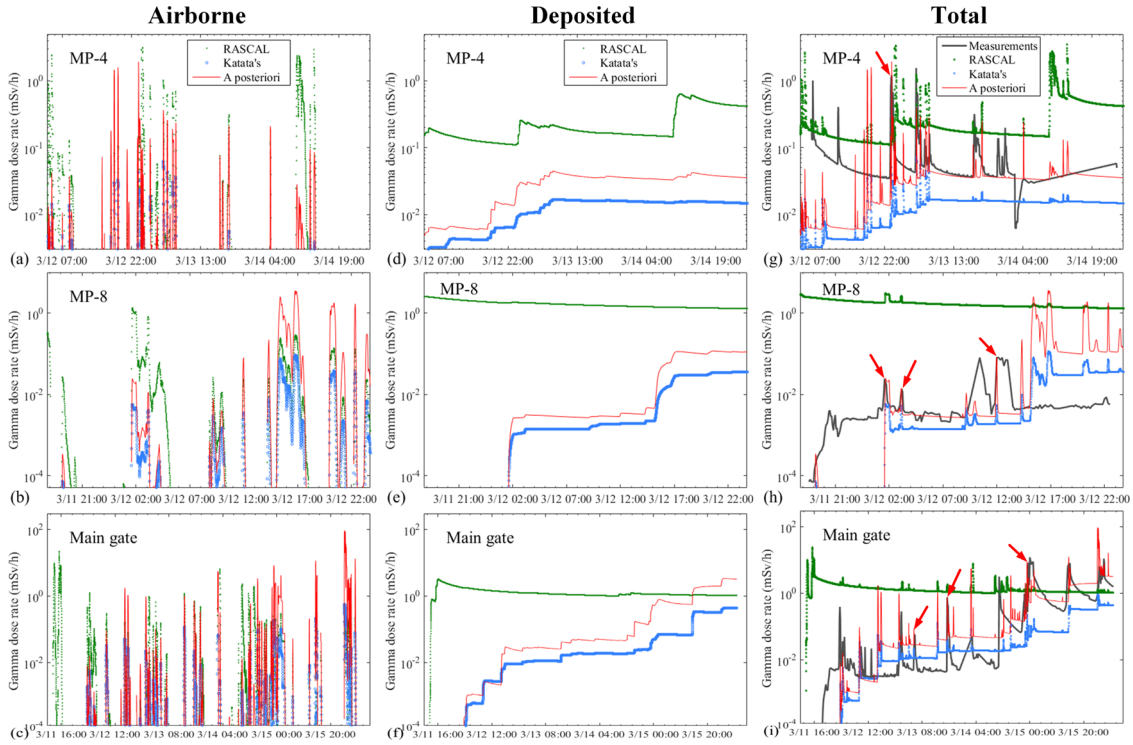

Fig. 5. Measured gamma dose rates and air dispersion model predictions using the RASCAL, Katata's, and a posteriori source term for MP-4, MP-8, and the main gate. The arrows indicate that the predicted peaks are close to those in the measurements.

$$\mathbf{z} = (\mathbf{R}_{Inv}\mathbf{X} + \mathbf{R}_{Rea}\mathbf{Y})\bullet\mathbf{c}_{Inv} \quad (4)$$

2.3. A priori release rate based on source inversion

This study uses Katata's source term estimate as the a priori information of release rates, because of its fine temporal details [8]. The four radionuclides (I-131, Cs-137, Cs-134, Te-132) in Katata's source term and their ratios form the first radionuclide group and the corresponding composition matrix $\mathbf{R}_{Inv}$ [8]. The release rate of Cs-137 in Katata's source term is used to form the a priori release rate $\mathbf{c}_{Inv}$.

2.4. A priori radionuclide composition based on reactor physics calculation

The Radiological Assessment System for Consequence Analysis (RASCAL) code is used to calculate the a priori radionuclide composition ($\mathbf{R}_{Rea}$) for the second group. This is based on the preset boil water reactor database and severe accident analysis results [13,14]. As calculation parameters, RASCAL uses a reactor power of 1380 MWt for Unit 1 and 2381 MWt for Units 2 and 3 [15]. The time that the core is uncovered, is estimated to be 2.5 h for Unit 1 and 4.5 h for Units 2 and 3 [16]. Following the Fukushima accident, the major releases occurred through the drywall, wetwall, and the building.

The RASCAL calculation provides a source term of 50 radionuclides, of which 23 contribute to more than 99% of the dose rate. Therefore, the release rates of these 23 radionuclides are the target of the estimation (Fig. 1). These radionuclides all emit gamma rays and make contribution to the on-site gamma dose rate measurement. The major contributors are Xe-133, Xe-135, I-131, I-132, and I-133, which have relatively short half-lives of between 2.3 h and 8.03 days. Fig. 1 compares the temporal variation of the above radionuclides, and shows that the composition of these radionuclides varies as the Fukushima accident progresses. Excluding the four radionuclides in Katata's source term (I-131, Cs-137, Cs-134, Te-132), the remaining 19 radionuclides and the corresponding ratios between their release rates are used to form the composition matrix of the second group ($\mathbf{R}_{Rea}$).

2.5. Numerical implementation

The matrix-vector multiplication $\mathbf{A}(\mathbf{R}\bullet\mathbf{c})$ gives the on-site air dispersion for the multi-radionuclide source input $\mathbf{R}\bullet\mathbf{c}$. The Lagrangian mesoscale atmospheric dispersion puff model, Risø Mesoscale PUFF (RIMPUFF), is used to perform the on-site simulations [17]. RIMPUFF calculates the concentration and dose rates for released radionuclides and takes radioactive decay as well as dry and wet deposition processes into consideration. The dry and wet deposition rates vary between different radionuclide groups [17]. In this study, the diffusion coefficients of RIMPUFF are upgraded to improve its performance over short distances [18].

The EnKF model [19–21] is used to determine the state vector $\begin{bmatrix}\mathbf{X}\\ \mathbf{Y}\end{bmatrix}$ from Eq. (3) for the whole measurement period, with the parameter settings taken from a previous study [22]. EnKF is an extended Kalman filter that describes the possible state and the corresponding error statistics of variables or model parameters using ensembles of random samples.

2.6. On-site gamma dose rate data preprocessing

Fig. 2 shows the temporal dose rate measurements at MP-4, MP-8, and the main gate. Three basic parts can be observed: a baseline, a peak, and a gradual decay. Among them, the peaks provide a clean record of the release events and their timing [12]. Thus, the source inversion in this study uses peak data only.

In order to reduce the uncertainties in the meteorological data, an air dispersion simulation with artificial constant release rates was performed, and the results (the red curve in Fig. 2) were compared with the dose rates measured on-site at FDNPP1. Because the release is constant, the timing of the peaks in the simulation (the red curve in Fig. 2) is determined purely by the meteorological field. The uncertainties in the meteorological field are minimal when the simulated peaks (red curve) coincide with those of the measurements. Therefore, only those peak dose rate data whose timing could be reproduced by

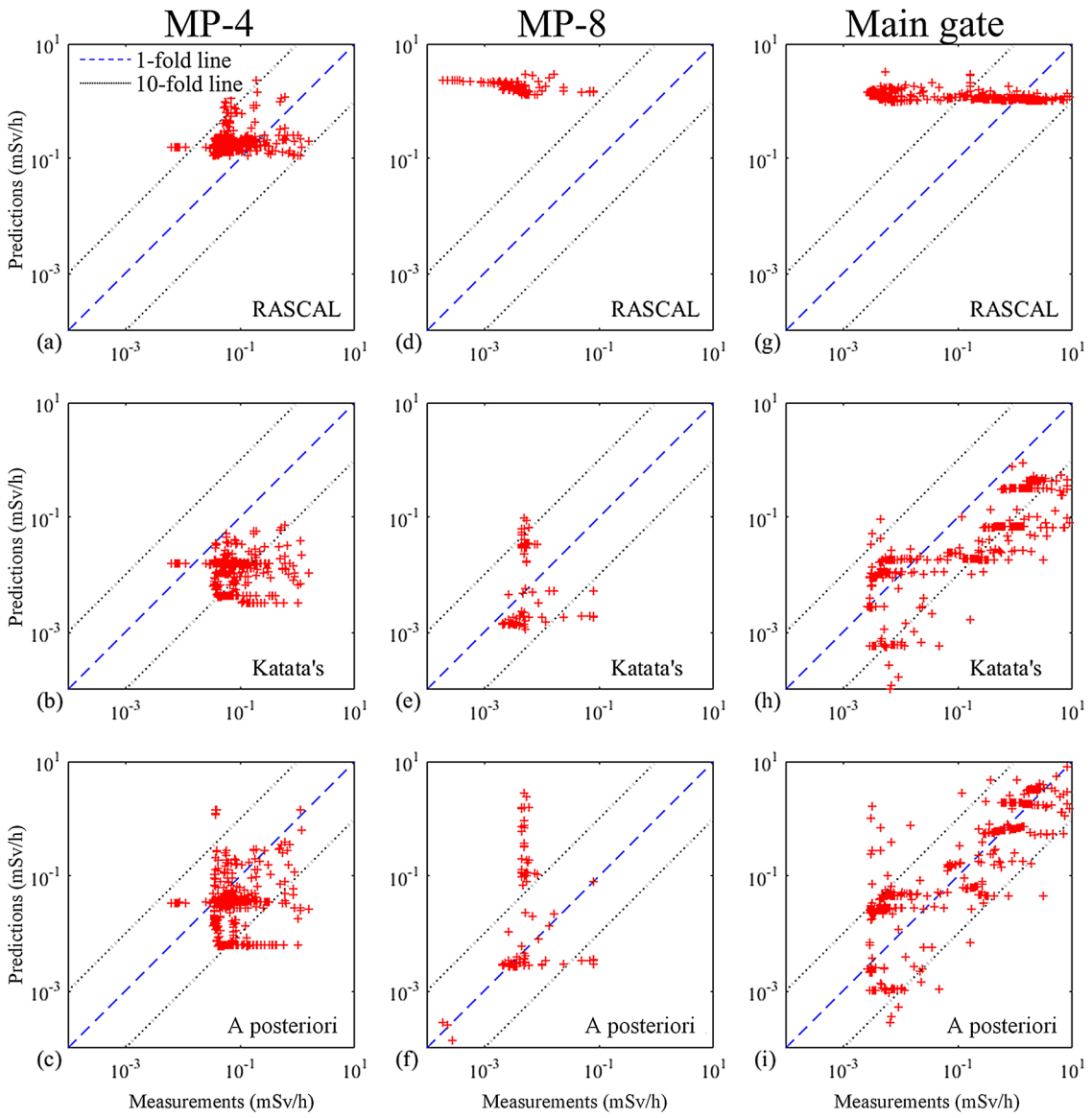

Fig. 6. Scatterplots for the on-site validation. From top to bottom: RASCAL, Katata's and a posteriori source term.

Table 1
Summary of performance measures for on-site validation using different source terms.

	RASCAL	Katata's	A posteriori
FAC2	0.12	0.07	0.46
FAC5	0.71	0.55	0.69
FAC10	0.76	0.78	0.91
MG	0.14	3.69	1.34
VG	1951.57	27.51	9.23

the simulation (indicated by the arrows in Fig. 2) were adopted to form the measurement vector μ in Eq. (3).

Although discrete in time, the selected data cover the duration of most release events (the blue and green shades in Fig. 2). Because it is reasonable to assume that the release is stable during each period [8], the weights remain constant over the duration of each event. This assumption ensures that the solution of Eq. (3) covers the whole measurement period.

3. Validation

3.1. On-site validation

The dose rate predictions using RASCAL, Katata's, and the a posteriori source term were compared with the measurements from MP-4, MP-8, and the main gate at FDNPP1 (Fig. 3a). MP-4, MP-8, and the main gate are located to the northwest, south, and southwest of the reactor, respectively. MP-4 and MP-8 are both ~1.2 km, whereas the main gate is ~1 km from the reactor. The parameters and settings of RIMPUFF were the same as those used for the source inversion.

3.2. Regional-scale validation

For the purpose of independent validation, WRF-Chem was used to simulate the regional Cs-137 dispersion and deposition based on RASCAL, Katata's and the a posteriori source term. The dry deposition was modeled with a constant deposition velocity of 0.05 cm s^{-1} [23]. For the wet deposition, in-cloud scavenging was modeled using the Roselle and Binkowski scheme [24] and below-cloud scavenging was modeled using the scheme of Baklanov and Sørensen [25]. The meteorological data generated by the non-hydrostatic model [26] and

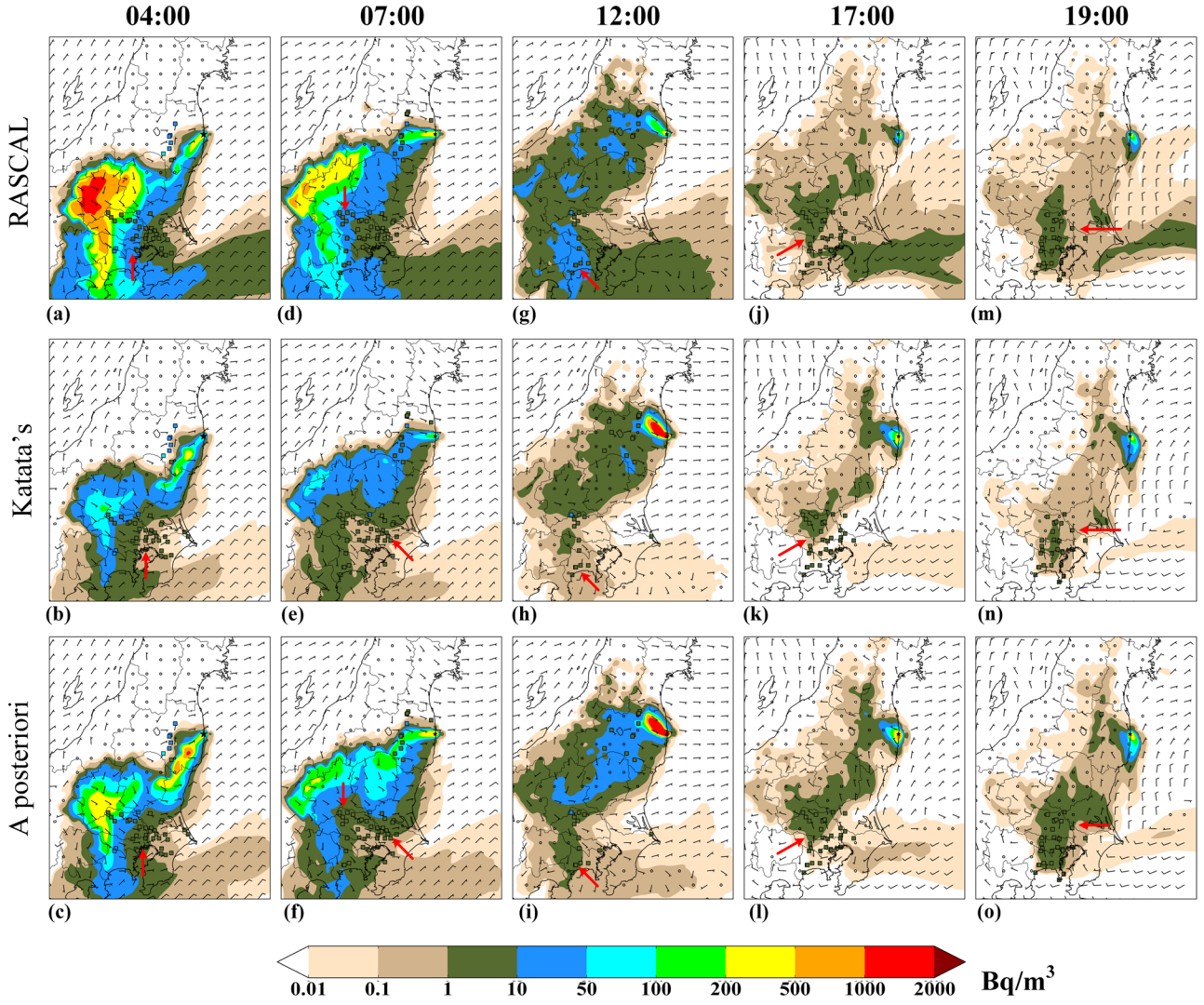

Fig. 7. Spatial distributions of the atmospheric concentration for different source terms for the period March 15–16. From top to bottom: RASCAL, Katata's and a posteriori source terms. The barbs represent the wind speed and wind direction, and the colored squares indicate the measurement sites. The arrows indicate representative differences in the predictions using the three source terms.

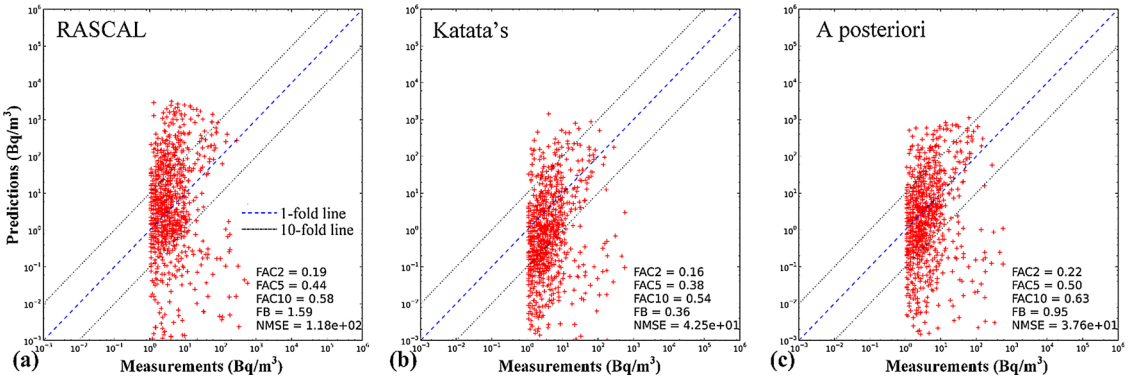

Fig. 8. Scatterplots for the whole regional-scale simulation period. (a): RASCAL source term; (b): Katata's source term; (c): A posteriori source term.

local ensemble Kalman filter [27,28] were used for the regional simulation. The spatial domain was constructed of 256 × 212 horizontal cells centered on 37.49 °N, 140.48 °E. The simulation period started at 00:00 UTC on March 11, 2011, and ended at 00:00 UTC on March 17, 2011. The simulation used 30 vertical levels, with the highest at the 10,000 Pa isobaric surface.

At the regional scale, the simulation results were compared with both the atmospheric concentration [10] and the cumulative deposition density of Cs-137 [29]. The site distribution is displayed in Fig. 3b.

3.3. Sensitivity to different a priori information

The proposed method was tested with three different combinations of a priori information:

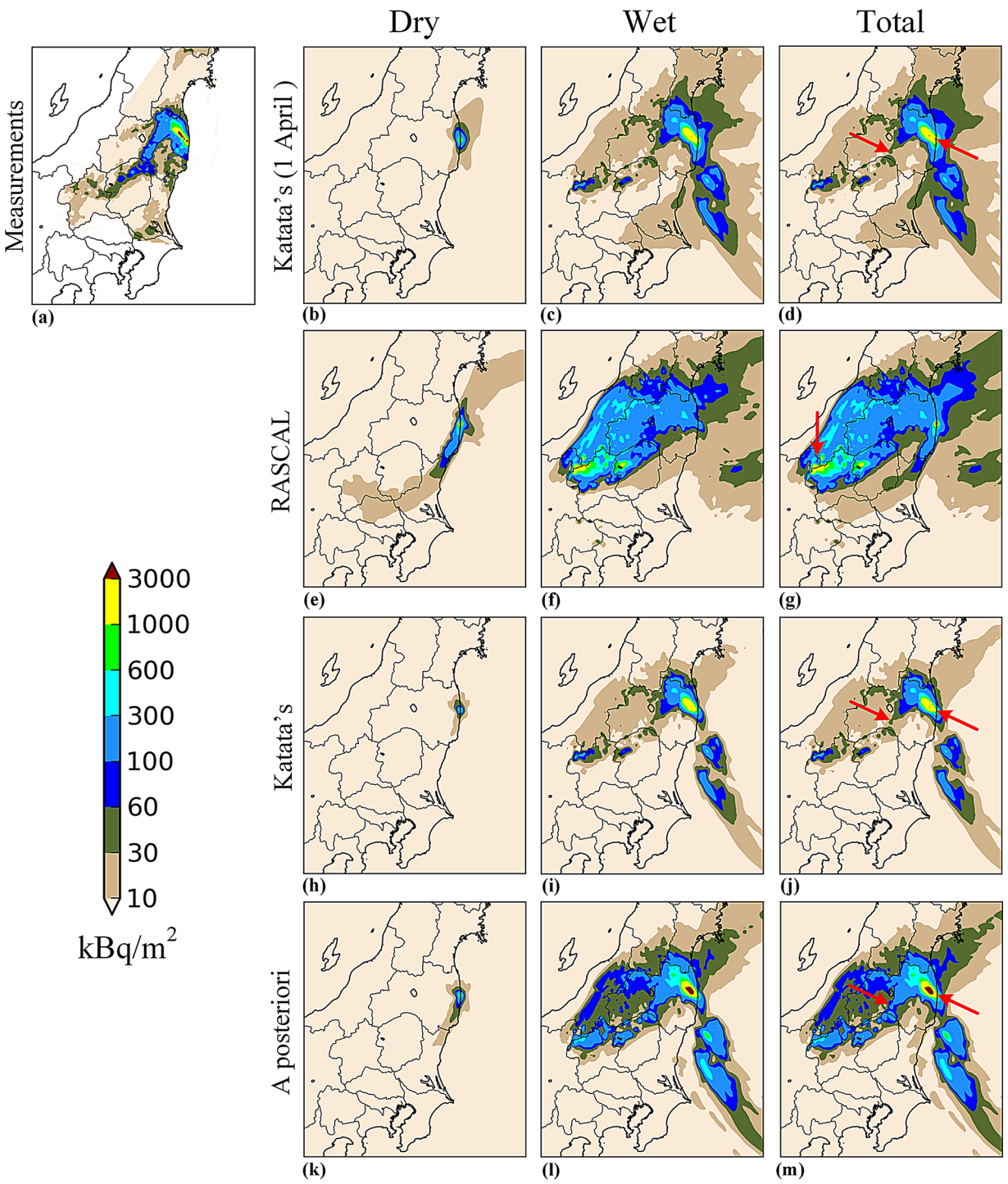

Fig. 9. Spatial distribution of surface deposition of Cs-137 using different source terms.

Table 2
Summary of performance measures for surface deposition of Cs-137 using different source terms.

	RASCAL	Katata's	A posteriori
FAC2	0.38	0.32	0.36
FAC5	0.73	0.62	0.79
FAC10	0.86	0.80	0.92
FB	0.36	−0.26	0.41
NMSE	9.58	5.34	4.26

1) TR case: Terada's source term [32] and the same RASCAL settings as for Fig. 1;
2) KRR case: Katata's source term and a more realistic RASCAL calculation with shorter venting and explosion durations;
3) KCR case: Katata's source term and a more conservative RASCAL setting with longer venting/explosion durations and higher leakage.

All of the settings and parameters of RIMPUFF and EnKF were as described in Sections 3.1 and 3.2.

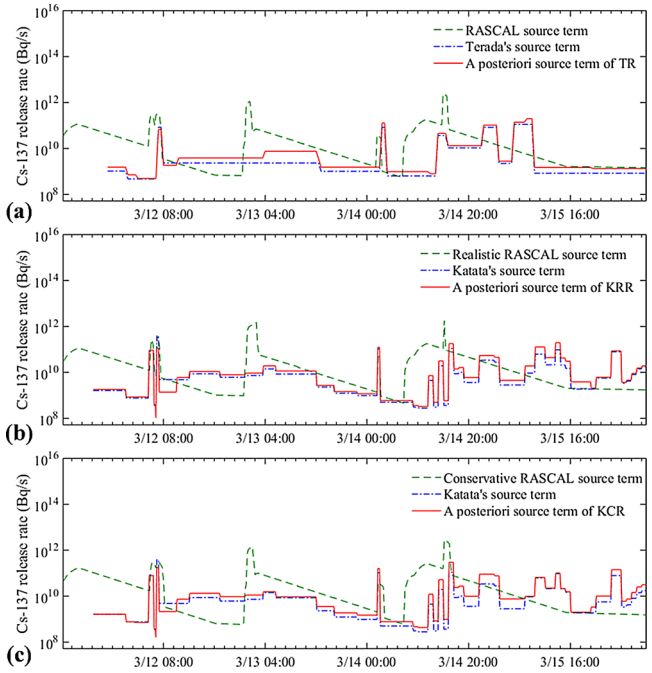

Fig. 10. Cs-137 release rate estimates of the three cases.

Table 3
Summary of performance measures for on-site validation using different source terms.

	TR case		KRR case		KCR case	
	Terada's	A posteriori	RASCAL	A posteriori	RASCAL	A posteriori
FAC2	0.11	0.32	0.10	0.44	0.09	0.45
FAC5	0.19	0.64	0.43	0.71	0.42	0.71
FAC10	0.48	0.80	0.76	0.87	0.75	0.86
MG	9.64	2.29	0.12	1.62	0.10	1.61
VG	846.83	18.97	3464.16	10.71	9078.00	11.24

3.4. Performance evaluation

Several quantitative metrics were used to evaluate the validation process [33–36], including the fraction of predictions within a factor of 2, 5, and 10 of the observations (FAC2, FAC5, and FAC10), geometric mean bias (MG), geometric variance (VG), fractional bias (FB), and normalized mean square error (NMSE) [33].

4. Results and discussion

4.1. RASCAL, Katata's source term, and a posteriori source term

Fig. 4a shows the weights given by Eq. (3). Both weights vary with time, indicating that the a priori release rate has different biases in different periods. Weights of less than 1 imply that the a priori release rate is overestimated at a specific time, and the weight corrects the overestimation in the final estimate. For weights above 1, an initial underestimation is corrected.

Fig. 4b compares the Cs-137 release rates. The release starts earlier with the RASCAL source term than with the other two, because the RASCAL model assumes leakage from the core being uncovered at 10:16 UTC on March 11. RASCAL and Katata's source term match well on the two peaks before 08:00 UTC on March 12 and one peak at 02:00 UTC on March 14, for which the discrepancy in peak values is within 70%. The first two peaks correspond to the U1 venting and explosion, and the final one corresponds to the U3 hydrogen explosion [8]. This consistency indicates that both methods agree well on the primary release events in the Fukushima accident. At about 02:00 UTC on March 13, RASCAL estimates a peak release that corresponds to drywell venting [16], but Katata's source term only slightly increases following this event. This inconsistency indicates that the two methods may differ in terms of secondary release events. For the non-peak release period, the RASCAL source term provides less detailed information than Katata's source term. The a posteriori source term has a similar temporal profile as Katata's source term. However, some details are different from Katata's source term, a result of the temporal variation of the weights (indicated by the arrows in Fig. 4b). For the period shown in Fig. 4, the total Cs-137 releases given by RASCAL and the a posteriori source term are 2.28×10^{16} Bq and 9.11×10^{15} Bq, respectively, whereas Katata's source term suggests a release of 5.20×10^{15} Bq [8].

Fig. 4c compares the release rates of I-131, which are all higher than their Cs-137 counterparts for the three source terms (Fig. 4b). The total I-131 release given by RASCAL, Katata's source term, and the a posteriori source term are 1.98×10^{17} Bq, 6.35×10^{16} Bq, and 1.06×10^{17} Bq, respectively. Despite this difference, the profile of the I-131 release is similar to that of Cs-137 for the three source terms.

Fig. 4d compares the I-133 release rates (note that this is not provided by Katata's source term). For the RASCAL source term, the three peaks before 04:00 UTC on March 14 are similar to those of I-131, but the other two peaks are lower than those of I-131 (Fig. 4c), indicating different behavior among radionuclides in the RASCAL source term. The a posteriori source term inherits both the detailed releases in Katata's source term and a slight decay trend that is similar to that of the RASCAL source term.

4.2. On-site validation

Fig. 5 compares the predicted airborne, deposited, and total dose rates at each site. For the airborne dose rate, the three predictions all show considerable peaks, in which the contribution of the short-lived radionuclides is over 90% (Fig. 5a–c). For the main gate (Fig. 5c), only the RASCAL prediction produces peaks before 14:00 UTC on March 11, because of its early start of release. For the same reason, the RASCAL deposited dose rate is higher than that given by the other two source terms in the early phase (the middle column of Fig. 5). For the deposited dose rates, the long-lived radionuclides make more than 80% contribution.

For the total dose rate (the right column of Fig. 5), the RASCAL predictions overestimate the baseline for most of the time at the three sites. Katata's source term produces mainly underestimations of the baseline at MP-4 and MP-8, but mainly overestimations at the main gate. Furthermore, the baseline exhibits no decaying trend, because Katata's source term does not contain any short-lived radionuclides. In contrast, the a posteriori source term improves the baseline for about the whole simulation period at MP-4, 1/2 of the period at MP-8, 1/3 of the period at the main gate. In terms of the peak values, the RASCAL predictions exhibit overestimations at MP-8, but show underestimations and overestimations at different times for MP-4 and the main gate. Katata's source term produces underestimations for most of the peaks at the three sites. Using the a posteriori source term, the predictions are close to the measurements for a number of peaks at the three sites (indicated by the arrows in Fig. 5g–i).

Fig. 6 compares the corresponding scatterplots. The RASCAL predictions generally give unsatisfactory correlation, and produce overestimations at MP-8 and the main gate. Katata's predictions exhibit better correlation than the RASCAL predictions, but produce underestimation for most measurements at MP-4 and the main gate. In comparison, the predictions using the a posteriori source term are more concentrated along the 1-fold line (Fig. 6i).

Table 1 summarizes several quantitative metrics for the on-site validation. Compared with the other two source terms, the predictions using the a posteriori source term exhibit better FAC2, FAC10, MG, and VG values. For FAC5, the performance of the a posteriori source term is

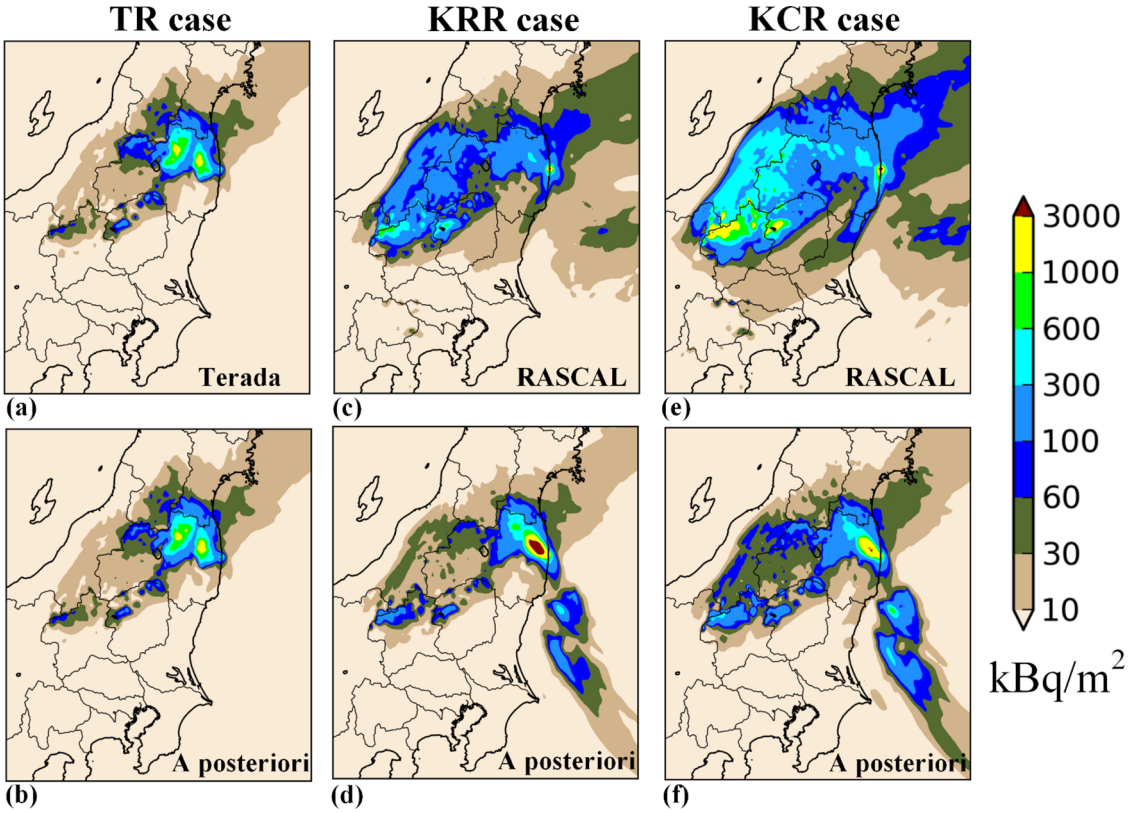

Fig. 11. Spatial distribution of surface deposition of Cs-137 in the three cases.

between that of RASCAL and Katata's source term.

4.3. Regional-scale validation

Fig. 7 compares the regional Cs-137 plume predictions for the period March 15–16, 2011. This period is chosen because the plume moved toward land, allowing most of the concentration data to be collected. At 04:00, 07:00, and 12:00 on March 15, the RASCAL source term results in overestimations in the west of the TMA, whereas Katata's source term introduces some underestimation in the east of the TMA. In comparison, the a posteriori source term alleviates the above two biases in the TMA (indicated by the arrows in the first three columns of Fig. 7). At other times, Katata's source term leads to some underestimation, whereas the RASCAL and a posteriori source terms better reproduce the medium concentration data (1–10 Bq/m^3) in the TMA (indicated by the arrows in the 4th and 5th columns of Fig. 7).

Fig. 8 compares the scatterplots of atmospheric concentrations for the whole simulation period of the regional-scale validation. The RASCAL source term produces an overestimation, whereas Katata's source term produces an underestimation (Fig. 8a and b). With the a posteriori source term, the above biases are reduced (Fig. 8c). Quantitatively, the RASCAL source term exhibits slightly better FACs, but worse FB and NMSE values than Katata's source term. The a posteriori source term produces the best metrics, except for FB.

Fig. 9 compares the cumulative dry, wet, and total deposition simulated using different source terms. The top row displays the measurements and a reference simulation using Katata's source term (up to April 1) and the parameters in section 3.2. All the predictions suggest that wet deposition is dominant in this accident. The RASCAL predictions give the largest area of deposition, but the spatial distribution exhibits significant deviation from the measurements, especially for the high-deposition area (indicated by the arrow in Fig. 9g). For Katata's source term, the dry and wet deposition (Fig. 9h–j) are fairly close to the reference simulation (Fig. 9b–d) in both the Nakadori area and the northwest of the FDNPP site, indicating that the deposition up to March 17 dominates the final deposition in these two areas. However, there are underestimations in the above areas (indicated by the arrows in Fig. 9d and j). For the a posteriori source term, the dry deposition is similar to that using Katata's source term. But, the wet and total deposition are closer to the measurements in the above two areas (Fig. 9m), although there are overestimations in the west of the Nakadori area.

Table 2 summarizes the quantitative metrics for the regional-scale cumulative deposition predictions. RASCAL gives good FACs, but has the worst NMSE, and the deviation in spatial distribution is not acceptable (Fig. 9g). Katata's source term produces moderate metrics. The a posteriori source term gives the best FAC5, FAC10, and NMSE scores, but its FB is worse than that with Katata's source term, mainly because of the overestimation in the west of the Nakadori domain.

4.4. Sensitivity analysis

Fig. 10a shows the source term estimates of the three combinations. Terada's source term indicates fewer release events than Katata's source term, and so the a posteriori source term also has fewer release events (Fig. 10a). The realistic and conservative RASCAL source terms produce differences in the width of the release peaks (Fig. 10b and c). The corresponding a posteriori source terms have similar release profiles, but slightly different release rates. Thus, the a posteriori source term is less sensitive to the RASCAL source term than the a priori reverse source term. This is because that the release rate of the RASCAL source term is not used in the proposed method.

Table 3 compares the quantitative metrics for the on-site validations. For all the test cases, the a posteriori method improves most of the metrics over the two a priori source terms. In addition, the metrics of the a posteriori source terms obtained with different RASCAL source terms show no significant differences, but the metrics of the a posteriori source terms obtained with Katata's source term are better than those

obtained with Terada's source term.

Fig. 11 compares the regional Cs-137 deposition simulations. For the TR case, the Terada and a posteriori source terms are visually similar (Fig. 11a and b). The two RASCAL source terms (Fig. 11c and e) exhibit considerable biases from the measurements in Fig. 9a. In comparison, the two corresponding a posteriori source terms make noticeable improvements (Fig. 11d and f). However, they differ in the Nakadori area and the northwest of the FDNPP site because of the different release rates on March 15, 2011 (Fig. 10b and c).

5. Conclusion

This paper has described a method that provides the source term for both long- and short-lived radionuclides based on long-overlooked on-site gamma dose rate data. The proposed method was validated against data obtained following the FDNPP1 accident. Using a weighted additive model, our method can handle conflicts between the priors obtained from different mechanisms, allowing these priors to be simultaneously incorporated into the source inversion process to reduce uncertainties. Such priors include the temporally varying multi-radionuclide composition calculated with the reactor physics code RASCAL and Katata's release rate estimate obtained through source inversion. In addition, a calibration simulation was performed to minimize the discrepancies between the air dispersion model and on-site measurements, further reducing the uncertainties. The resulting a posteriori source term was validated by both on-site gamma dose rates and regional-scale Cs-137 measurements. The results demonstrate that the a posteriori source term successfully combines the details of long-lived radionuclide release rates in Katata's source term and the temporal variation of short-lived radionuclides in the RASCAL calculations. The sensitivity analysis indicates that the a posteriori source term is less sensitive to the RASCAL calculation than to the a priori reverse source term. Given different combinations of the a priori source terms, this allows the model predictions of the on-site gamma dose rates to be improved. With a detailed a priori reverse source term, the a posteriori source term significantly improves the model predictions of the on-site gamma dose rates. Additionally, it substantially enhances the accuracy of model predictions for both atmospheric concentrations and the cumulative deposition pattern at the regional scale compared with the two a priori source terms. Given such improvements, the proposed method provides a framework for the source inversion of both long- and short-lived radionuclide releases.

Acknowledgements

This work is supported by the National Natural Science Foundations of China [grant number 11875037, 11475100]. We thank the editors and reviewers, for their valuable comments, which substantially improves the quality of this paper.

References

[1] J.E. Ten Hoeve, M.Z. Jacobson, Worldwide health effects of the Fukushima Daiichi nuclear accident, Energy Environ. Sci. 5 (2012) 8743–8757.
[2] R. Addis, G. Fraser, F. Girardi, G. Graziani, Y. Inoue, N. Kelly, W. Klug, A. Kulmala, K. Nodop, J. Pretel, ETEX: a European tracer experiment; observations, dispersion modelling and emergency response, Atmos. Environ. 32 (1998) 4089–4094.
[3] O. Saunier, A. Mathieu, D. Didier, M. Tombette, D. Quélo, V. Winiarek, M. Bocquet, An inverse modeling method to assess the source term of the Fukushima nuclear power plant accident using gamma dose rate observations, Atmos. Chem. Phys. 13 (2013) 11403–11421.
[4] A. Stohl, P. Seibert, G. Wotawa, D. Arnold, J.F. Burkhart, S. Eckhardt, C. Tapia, A. Vargas, T.J. Yasunari, Xenon-133 and caesium-137 releases into the atmosphere from the Fukushima Dai-ichi nuclear power plant: determination of the source term, atmospheric dispersion, and deposition, Atmos. Chem. Phys. 12 (2012) 2313–2343.
[5] K. Yumimoto, Y. Morino, T. Ohara, Y. Oura, M. Ebihara, H. Tsuruta, T. Nakajima, Inverse modeling of the137Cs source term of the Fukushima Dai-ichi Nuclear Power Plant accident constrained by a deposition map monitored by aircraft, J. Environ. Radioact. 164 (2016) 1–12.
[6] M. Chino, H. Nakayama, H. Nagai, H. Terada, G. Katata, H. Yamazawa, Preliminary estimation of release amounts of 131I and 137Cs accidentally discharged from the Fukushima Daiichi Nuclear Power Plant into the atmosphere, J. Nucl. Sci. Technol. 48 (2012) 1129–1134.
[7] G. Katata, M. Ota, H. Terada, M. Chino, H. Nagai, Atmospheric discharge and dispersion of radionuclides during the Fukushima Dai-ichi Nuclear Power Plant accident. Part I: Source term estimation and local-scale atmospheric dispersion in early phase of the accident, J. Environ. Radioact. 109 (2012) 103–113.
[8] G. Katata, M. Chino, T. Kobayashi, H. Terada, M. Ota, H. Nagai, M. Kajino, R. Draxler, M.C. Hort, A. Malo, T. Torii, Y. Sanada, Detailed source term estimation of the atmospheric release for the Fukushima Daiichi Nuclear Power Station accident by coupling simulations of an atmospheric dispersion model with an improved deposition scheme and oceanic dispersion model, Atmos. Chem. Phys. 15 (2015) 1029–1070.
[9] V. Winiarek, M. Bocquet, N. Duhanyan, Y. Roustan, O. Saunier, A. Mathieu, Estimation of the caesium-137 source term from the Fukushima Daiichi nuclear power plant using a consistent joint assimilation of air concentration and deposition observations, Atmos. Environ. 82 (2014) 268–279.
[10] Y. Oura, M. Ebihara, H. Tsuruta, T. Nakajima, T. Ohara, M. Ishimoto, H. Sawahata, Y. Katsumura, W. Nitta, A database of hourly atmospheric concentrations of radiocesium (134 Cs and 137 Cs) in suspended particulate matter collected in March 2011 at 99 air pollution monitoring stations in Eastern Japan, J. Nucl. Radiochem. Sci. 15 (2015) 15–26.
[11] H. Tsuruta, Y. Oura, M. Ebihara, T. Ohara, T. Nakajima, First retrieval of hourly atmospheric radionuclides just after the Fukushima accident by analyzing filter-tapes of operational air pollution monitoring stations, Sci. Rep. 4 (2014).
[12] A. Dvorzhak, C. Puras, M. Montero, J.C. Mora, Spanish experience on modeling of environmental radioactive contamination due to Fukushima Daiichi NPP accident using JRODOS, Environ. Sci. Technol. (2012).
[13] T.J. McKenna, J.G. Giitter, Source Term Estimation During Incident Response to Severe Nuclear Power Plant Accidents, NUREG-1228, Washington DC, 1988.
[14] USNRC, Accident Source Terms for Light-water Nuclear Power Plants, NUREG-1465, Washington DC, 1995.
[15] S. Uchida, M. Naitoh, H. Suzuki, H. Okada, Evaluation of accumulated fission products in the contaminated water at the Fukushima Daiichi Nuclear Power Plant, Nucl. Technol. 5450 (2014).
[16] A. Guglielmelli, F. Rocchi, FAST-1: Evaluation of the Fukushima Accident Source Term Through the Fast Running Code RASCAL 4.2: Methods & Results, Centro Ricerche Bologna, Washington DC, 2014.
[17] S. Thykier-Nielsen, S. Deme, T. Mikkelsen, Description of the Atmospheric Dispersion Module RIMPUFF, Risø National Laboratory, Roskilde, Denmark, 1999.
[18] Y. Liu, H. Li, S. Sun, S. Fang, Enhanced air dispersion modelling at a typical Chinese nuclear power plant site: coupling RIMPUFF with two advanced diagnostic wind models, J. Environ. Radioact. 175–176 (2017) 94–104.
[19] G. Evensen, Sequential data assimilation with a nonlinear quasi-geostrophic model using Monte Carlo methods to forecast error statistics, J. Geophys. Res. Ocean 99 (C5) (1994) 10143–10162.
[20] G. Evensen, Advanced data assimilation for strongly nonlinear dynamics, Mon. Weather Rev. 125 (1997) 1342–1354.
[21] G. Evensen, The Ensemble Kalman Filter: theoretical formulation and practical implementation, Ocean Dyn. 53 (2003) 343–367.
[22] S. Sun, H. Li, S. Fang, A forward-backward coupled source term estimation for nuclear power plant accident: a case study of loss of coolant accident scenario, Ann. Nucl. Energy 104 (2017) 64–74.
[23] X. Hu, D. Li, H. Huang, S. Shen, E. Bou-Zeid, Modeling and sensitivity analysis of transport and deposition of radionuclides from the fukushima dai-ichi accident, Atmos. Chem. Phys. 14 (2014) 11065–11092.
[24] S.J. Roselle, F.S. Binkowski, D.W. Byun, J.K.S. Ching (Eds.), Cloud Dynamics and Chemistry, in: Science algorithms of the EPA Models-3 Community multiscale air quality (CMAQ) modeling system, US Environmental Protection Agency, Washington, DC, 1999.
[25] A. Baklanov, J.H. Sørensen, Parameterisation of radionuclide deposition in atmospheric long-range transport modelling, Phys. Chem. Earth, Part B Hydrol. Ocean. Atmos. 26 (2001) 787–799.
[26] K. Saito, T. Fujita, Y. Yamada, J. Ishida, Y. Kumagai, K. Aranami, S. Ohmori, R. Nagasawa, S. Kumagai, C. Muroi, T. Kato, H. Eito, Y. Yamazaki, The operational JMA nonhydrostatic mesoscale model, Mon. Weather Rev. 134 (2006) 1266–1298.
[27] T.T. Sekiyama, M. Kajino, M. Kunii, The impact of surface wind data assimilation on the predictability of near-surface plume advection in the case of the Fukushima Nuclear accident, J. Meteorol. Soc. Japan. Ser. II. 95 (2017) 447–454.
[28] T.T. Sekiyama, M. Kunii, M. Kajino, T. Shimbori, Horizontal resolution dependence of atmospheric simulations of the fukushima nuclear accident using 15-km, 3-km, and 500-m grid models, J. Meteorol. Soc. Japan. Ser. II. 93 (2015) 49–64.
[29] NRA, Readings of Seawater and Dust Monitoring in Sea Area by MEXT (March 2011), (2011) (Accessed 12 November 2014), http://radioactivity.nsr.go.jp/en/list/259/list-201103.html.
[30] TEPCO, Radiation Dose Measured in the Fukushima Daiichi Nuclear Power Station, (2011) (Accessed 18 November 2011), http://www.tepco.co.jp/en/nu/fukushima-np/f1/index-e.html.
[31] Y. Sato, M. Takigawa, T. Sekiyama, M. Kajino, H. Terada, H. Kondo, J. Uchida, D. Goto, D. Quélo, A. Mathieu, A. Quérel, S. Fang, Y. Morino, P. von Schoenberg, H. Grahn, N. Brännström, S. Hirao, H. Tsuruta, H. Yamazawa, T. Nakajima, Model intercomparison of atmospheric 137Cs from the Fukushima Daiichi Nuclear Power Plant accident: simulations based on identical input data, J. Geophys. Res. Submitted (2018) 748–765.
[32] H. Terada, G. Katata, M. Chino, H. Nagai, Atmospheric discharge and dispersion of radionuclides during the Fukushima Dai-ichi Nuclear Power Plant accident. Part II:

verification of the source term and analysis of regional-scale atmospheric dispersion, J. Environ. Radioact. 112 (2012) 141–154.
[33] J.C. Chang, S.R. Hanna, Air quality model performance evaluation, Meteorol. Atmos. Phys. 87 (2004) 167–196.
[34] S.R. Hanna, Confidence limits for air quality model evaluations, as estimated by bootstrap and jackknife resampling methods, Atmos. Environ. 23 (1989) 1385–1398.
[35] J.C. Chang, Methodologies for Evaluating Performance and Assessing Uncertainty of Atmospheric Dispersion Models, (2003).
[36] J.C. Chang, P. Franzese, K. Chayantrakom, S.R. Hanna, Evaluations of CALPUFF, HPAC, and VLSTRACK with two mesoscale field datasets, J. Appl. Meteorol. Climatol. 42 (2003) 453–466.